Cation Selectivity by the CorA Mg^{2+} Channel Requires a Fully Hydrated Cation[†]

Andrea S. Moomaw[*] and **Michael E. Maguire**
Department of Pharmacology, School of Medicine, Case Western Reserve University, Cleveland, OH 44106-4965

Abstract

The CorA Mg^{2+} channel is the primary uptake system in about half of all bacteria and archaea. However, the basis for its Mg^{2+} selectivity is unknown. Previous data suggested that CorA binds a fully hydrated Mg^{2+} ion, unlike other ion channels. The crystal structure of *Thermotoga maritima* CorA shows a homopentamer with two transmembrane segments per monomer connected by a short periplasmic loop. This highly conserved loop, ^{281}EFMPELKWS^{289} in *Salmonella enterica* serovar Typhimurium CorA, is the only portion of the channel outside of the cell, suggesting a role in cation selectivity. Mutation of charged residues in the loop, E281 and K287, to any of several amino acids had little effect, demonstrating that despite conservation, electrostatic interactions with these residues are not essential. While mutation of the universally conserved E285 gave a minimally functional channel, E285A and E285K mutants were the most functional, again indicating that the negative charge at this position is not a determining factor. Several mutations at K287 and W288 behaved anomalously in a transport assay. Analysis indicated that mutation of K287 and W288 disrupts cooperative interactions between distinct Mg^{2+} binding sites. Overall, these results are not compatible with electrostatic interaction of the Mg^{2+} ion with the periplasmic loop. Instead, the loop appears to form an initial binding site for *hydrated* Mg^{2+}, not for the dehydrated cation. The loop residues may function to accelerate dehydration of the before entry of Mg^{2+} into the pore of the channel.

Magnesium is an essential cation required for numerous cellular functions, including coordination to nucleotide triphosphates, membrane stability, regulation of gene transcription, DNA replication, enzyme catalysis and protein synthesis (1–5). Deficiencies in Mg^{2+} result in a number of pathological disease states and in turn can promote deficiencies in other important cations such as Ca^{2+} and K$^+$ (6–12). The ubiquitous involvement of Mg^{2+} in important biological processes makes it a critical cation for study.

As with any cation, transmembrane entry pathways are required. Bacterial and Archaeal species have at least three different Mg^{2+} uptake systems. Enterobacteria and a few other groups of bacteria express the P-type ATPases MgtA and MgtB under low Mg^{2+} conditions (13–15). However, the primary route for Mg^{2+} entry is through either the CorA or the MgtE Mg^{2+} channel. Either CorA or MgtE appear to be present in all fully sequenced bacterial and archaeal genomes. Approximately half of bacterial and archaeal genomes contain the CorA

[*]Corresponding Author: Andrea S. Moomaw, Department of Pharmacology, School of Medicine, Case Western Reserve University, 2109 Adelbert Rd Wood Building, Cleveland, OH 44106-4965, Phone: 216-368-6187, Fax: 216-368-1300, andrea.moomaw@case.edu.

Supporting Information Available

Supporting information is available free of charge online at http://pubs.acs.org. Supplemental information includes sequence alignments and Western blots to show protein expression, localization and membrane assembly of CorA.

Mg^{2+} channel while the other half expresses the MgtE Mg^{2+} channel (16;17). A few species express both channels.

The crystal structures of the *Thermotoga maritima* CorA (18–20) and *Thermus thermophilus* MgtE (21) Mg^{2+} channels have been recently determined. MgtE, whose eukaryotic homologs are the SLC41A family of transport systems (22), is a homodimer with a total of 10 transmembrane (TM) segments and a modular bipartite cytosolic domain (21). The CorA Mg^{2+} channel's primary eukaryotic homolog is the mitochondrial Mrs2 Mg^{2+} channel. CorA is a homopentamer with two transmembrane segments (TM1 and TM2) per monomer. Its large N-terminal domain and the short 6 residue C-terminus are cytosolic. CorA crystal structures suggest that the pore of the protein is formed solely by TM1 (18–20).

Opening of the channel appears to be controlled by Mg^{2+} occupation of metal binding sites in the cytosolic domain. These Mg^{2+} ions have been hypothesized to act as "Mg^{2+} sensors" such that their dissociation from CorA allows movement of the monomers, opening the channel (18–20). Molecular dynamics simulations support this interpretation (23). An even more extensive set of bound Mg^{2+} ions in the cytosolic domain of the MgtE Mg^{2+} channel appears to provide a similar function. Mutagenesis and electrophysiological analysis strongly support such a role for the bound Mg^{2+} in MgtE (21;24).

The periplasmic end of TM1 contains the highly conserved 'YGMNF' motif. Mutations in this motif abolish Mg^{2+} transport, indicating that it is essential for function (25). Both TM segments are comprised solely of uncharged generally nonpolar amino acids. The pore appears to be lined only with backbone carbonyl groups. The few Ser and Thr residues in the membrane domain do not appear to contribute their hydroxyl groups to the pore (25). Thus, membrane flux of the most charge dense of the biological cations does not involve electrostatic interactions with the cation. This conclusion is supported by recent molecular dynamics simulations of CorA (23).

The transmembrane segments are connected through the periplasm by a short, charged 9 amino acid loop. This periplasmic loop was unresolved in all reported crystal structures, most likely due to a high degree of flexibility (18–20). Because the loop is the only portion of CorA exposed on the exterior membrane face, it is logical to hypothesize that it is involved in the initial interaction of the channel with substrate cations and likely participates in cation selectivity, but the mechanism of selectivity has not been explored in any depth.

Understanding the mechanism of Mg^{2+} selectivity with its transporters and channels necessitates consideration of the unique chemistry of the Mg^{2+} cation (17;26). Hydrated Mg^{2+} is the largest of all biological cations at 5 Å in diameter, almost twice the diameter of hydrated Ca^{2+}. The atomic ion however is among the smallest of all cations at 0.65 Å. Consequently, Mg^{2+} undergoes a much larger change in volume from hydrated cation to atomic ion than any other cation, 400-fold *versus* 4–25-fold changes in volume for Na^+, K^+ or Ca^{2+}. Mg^{2+} is invariably hexacoordinate. By contrast, Ca^{2+} can have several coordination states. Mg^{2+} holds its waters of hydration 10^3–10^4 more tightly than Ca^{2+}, Na^+ and K^+. These properties result in a rigid octahedral structure in which 90 degree bond angles are strongly preferred. The rate of exchange of the waters of hydration of Mg^{2+} is only 10^5/sec, compared to ~10^9 for other biological cations (Figure 1) (27). This unique chemistry suggests that channels and transporters interacting with Mg^{2+} may have properties distinct from those of other ion transport systems (17;19;26;28).

Recent electrophysiological experiments with the eukaryotic CorA Mg^{2+} channel homolog Mrs2 (29) and the bacterial MgtE Mg^{2+} channel (30) support this supposition. Both are ion channels with surprisingly high conductances of ~90–150 pS. Preliminary data with *S.* Typhimurium CorA suggests a similarly high conductance of ~140 pS (C. Obejero-Paz, A.

Moomaw, S.W. Jones and M.E. Maguire, unpublished). A conductance of this magnitude indicates a flux rate $>10^7$ ions/sec through these two classes of Mg^{2+} channels. This rate is at least 2 orders of magnitude greater than the exchange rate of the waters of hydration surrounding Mg^{2+} (Figure 1) (26), an indication that the typical aqueous chemistry of Mg^{2+} cannot explain the measured conductance of these channels.

Thus, any hypothesis concerning the mechanism of the CorA Mg^{2+} channel must explain not only cation selectivity but also the anomalously high conductance. Our previous work identifying cobalt(III) hexaammine (CoHex) as a selective competitive inhibitor of CorA (31) provides a starting point for investigation. Crystal structures of CoHex and similar compounds such as Ru(II) and Ru(III) hexaammine (32) show that they are comparable in size to a hydrated Mg^{2+} cation, ~5Å. Because the ammine groups are covalently linked to Co^{2+} and therefore stable, these compounds represent structural analogs of the fully hydrated Mg^{2+} cation. Their ability to selectively inhibit CorA suggests that CorA initially interacts with a fully hydrated Mg^{2+} ion. The data presented in this report show that electrostatic interactions between charged residues of the periplasmic loop and the atomic (unhydrated) substrate ion do not occur. Rather, the loop (and possibly an external portion of the pore) interacts only with the fully hydrated cation. This could allow the channel to facilitate dehydration, thus allowing a partially hydrated Mg^{2+} to enter the pore. Thus, a significant part of the selectivity of CorA for Mg^{2+} derives from binding the fully hydrated cation.

Experimental Procedures

Mutagenesis

Site-directed mutagenesis was carried out using non-overlapping $5'-PO_4$ primers (Sigma Aldrich). Mutagenesis was carried out in DH5α *E. coli* cells using the pOK12 vector (33), obtained from Dr. Patrick Viollier, University of Geneva. After mutants were confirmed by sequencing (Biotic Solutions, New York, NY), the gene was transferred into the pBADB*myc*/His vector (Invitrogen) using BglII and EcoRI restriction sites. The pBAD vector was modified so that the *myc*/His tag is not expressed because a C-terminal tag greatly diminishes expression. Mutants were passaged through the restrictionless *S.* Typhimurium strain JR501 before being transformed into the Mg^{2+} dependent *S.* Typhimurium strain MM281 (*corAmgtA mgtB*) (34).

Cation transport assay

CorA mediated ion flux was measured using $^{63}Ni^{2+}$ (Brookhaven National Laboratory, Upton, NY and Eckert & Ziegler, Inc., Valencia, CA) or $^{57}Co^{2+}$ (MP Biomedical, Solon, OH) using previously described methods (35;36). $^{28}Mg^{2+}$ is not used because of its prohibitive expense. Strains from frozen stock were grown overnight in LB broth with 6 μg/ μl ampicillin and 100 mM $MgSO_4$. Cells were then subcultured in N-minimal media (37) supplemented with 0.01% casamino acids, 100 mM $MgSO_4$ and 1 mM L-arabinose or in LB broth supplemented with 100 mM $MgSO_4$ and 1 mM L-arabinose. The L-arabinose serves both as a carbon source for growth as well as the inducing agent for transcription of *corA* from the pBAD vector. At an OD_{600nm} ~ 0.4, cells were centrifuged at 3220 x *g* for 10 min at 4°C and washed twice with cold N-minimal media to remove extracellular Mg^{2+}. From this point, cells were kept on ice and buffers were ice cold. Unless otherwise noted, uptake assays used final concentrations of 100–200 μM Ni^{2+} or 20 μM Co^{2+} which approximates the concentration needed for half maximal uptake (34;38). The standard reaction contained 0.1–0.2 OD_{600nm} units of cells in N-minimal media containing 100 μM $NiCl_2$ (or 20 μM $CoCl_2$), ~300–600 nCi $^{63}Ni^{2+}$ (unless noted differently) and the indicated concentration of competing cation in a final volume of 1 ml. Uptake was measured for 10 min at 37°C before

dilution with 4 ml of ice-cold wash buffer (N-minimal medium, 10 mM Mg^{2+}, 1 mM EDTA) and immediate filtration through Protran BA85 0.45 µm filters (Whatman, Dassel, Germany). Filters were washed twice with an additional 4 ml of wash buffer, dissolved in 5 ml of Bio-Safe II (Research Products International, Mt. Prospect, IL) and counted in a scintillation counter. Efficiency was ~80% for $^{63}Ni^{2+}$ and ~100% for $^{57}Co^{2+}$. These transport experiments measure the concentration of cation required to half maximally inhibit the influx of the radioisotopic tracer cation, which is termed an apparent cation affinity. Transport probes whether individual residues are involved directly or indirectly in cation binding. However, this cannot be interpreted as an actual affinity of the cation for a specific binding site since cation flux involves interactions of the cation with multiple parts of the channel.

Growth complementation

Strains were grown overnight at 37°C in LB with 6 µg/µl ampicillin and 100 mM $MgSO_4$ before subculture into N-minimal media supplemented with 0.01% casamino acids, 1 mM L-arabinose and 100 mM $MgSO_4$ and overnight growth at 37°C. Cultures were centrifuged 10 min at $3220 \times g$ and washed twice with room temperature N-minimal media without supplements before resuspension in the original volume of N-minimal medium. A 96-well plate was set up with 12 concentrations of $MgSO_4$ from 0.01 mM to 10 mM. The plate format allowed testing of four strains in triplicate. MM3430, expressing wild type CorA from the same vector in MM281, was included on all plates as a control. Each strain was inoculated at an $OD_{600nm} = 0.05$. The volume in each well was adjusted to 50 µl using un-supplemented N-minimal media. An additional 200 µl of supplemented N-minimal media containing 0.01% casamino acids and 1 mM L-arabinose was added to each well for a final volume of 250 µl. The plate was incubated overnight at 37°C in a Molecular Devices Versamax microplate reader (Sunnyvale, CA) with shaking. The OD_{600nm} was measured every 20 min for 14 hr.

Cell fractionation

Cell fractionation was adapted from the protocol in Fraser *et al*. (39). Cells were grown overnight, sub-cultured into 7 ml LB media with 6 µg/µl ampicillin and 100 mM $MgSO_4$ and grown for two hours before protein induction with 1 mM L-arabinose. Protein expression was induced for 1–1.5 hours. Cells were centrifuged for 5 min at $10,000 \times g$, 4°C. Cells were resuspended in freshly made Buffer 1 (30 mM Tris-HCl, pH 8.0, 20% w/v sucrose, 1 mM EDTA). Cells were incubated with 1 mg/ml lysozyme (Sigma) for 10 min on ice and then sonicated $3 \times$ for 10–15 sec using a Branson Sonifier® 150 with a microtip, keeping cells on ice between each sonication. Cells were then spun at $12,000 \times g$ for 10 min at 4°C. The supernatant was considered the periplasmic fraction. The pellet was resuspended in Buffer 2 (0.1 M Tris-HCl, pH 8.0, 1 mM EDTA) and incubated with 10 µg/ml DNase I (Sigma) for 30 min on ice. After centrifugation at $12,000 \times g$ for 10 min at 4°C, the supernatant was removed. This was considered the cytoplasmic fraction. The pellet was resuspended in Buffer 3 (50 mM Tris-HCl, pH 8.0, 100 mM NaCl, 1.0% w/v Triton X-100, 10 mM EDTA) and incubated on ice for 15 min. The solubilized pellet was centrifuged at $12,000 \times g$ for 15 min at 4°C. The supernatant was considered the solubilized membrane fraction. The remaining pellet was considered as an insoluble fraction potentially containing inclusion bodies. After washing the pellet with 100 µl of sterile H_2O, it was stored at −20°C or solubilized for immediate use. The fraction was solubilized by resuspension in Buffer 4 (8 M urea in 25 mM Tris-HCl, pH 8.0, 1 mM DTT (Fisher)) and incubated at room temperature for 10 min before centrifugation at $12,000 \times g$ for 5 min at 4°C, retaining the supernatant. Protein was measured using the Bio-Rad Protein Assay (Hercules, California). An equal amount of protein from each fraction was run on an SDS-PAGE gel and analyzed for CorA by Western blot.

Formaldehyde crosslinking

Formaldehyde crosslinking was performed as previously described by Warren *et al*. (40). Mutants were grown overnight at 37°C in LB broth with 100 mM $MgSO_4$. Cells were subcultured in LB with 100 mM $MgSO_4$. After 2 hr growth, protein expression was induced with 1 mM L-arabinose. When cells reached an OD_{600nm} of ~0.5, 12 ml of cells were pelleted at 3220 x g for 10 min. Cells were resuspended in 12 ml of 0.1 M sodium phosphate buffer, pH 6.8, and 37% formaldehyde was added to a final concentration of 1% (v/v). After incubation for 5 min at room temperature, cells were pelleted at 3220 x g for 10 min. The pellet was resuspended in 5X non-reducing SDS-PAGE sample buffer, incubated at 60°C for 10 min and run on a 10% acrylamide non-reducing gel. CorA was visualized by Western blot analysis as previously described using a polyclonal antibody against the N-terminal 15 amino acids (41).

Results

Salmonella versus Thermotoga *CorA*

As shown in Supplemental Figure 1A, the sequences of *T. maritima* CorA and *S.* Typhimurium CorA are almost identical in the membrane domain and extracellular loop; differences between the two CorA channels are all conservative, hydrophobic substitutions. Consequently, their structures can reasonably be assumed to be almost identical in this region, allowing direct comparison of the *S.* Typhimurium CorA functional data with the *T. maritima* CorA structure. Amino acid numbering is for *S.* Typhimurium CorA except as noted. Adding 35 to the *S.* Typhimurium residue number gives the *T. maritima* residue number.

Expression, growth and assembly of mutants

To facilitate comparison between wild type and mutant CorA channels, strains should express similar levels of CorA protein. Unless otherwise noted, all mutant CorA channels expressed at levels similar to wild type CorA expressed from the same pBAD plasmid (Supplemental Figure 2 and data not shown). Wild type and all mutant strains were tested for inclusion body formation and for insertion of CorA into the membrane as described in Methods. For most mutants, there was little or no CorA protein in the inclusion body fraction (data not shown); however, some mutants did show some CorA protein in the inclusion body fraction (Supplemental Figure 3 and data not shown). The amount of protein in the inclusion body fraction was highly variable but was never greater than the level in the membrane fraction.

Because expression levels of the mutants were comparable to wild type expression, levels of total $^{63}Ni^{2+}$ (or $^{57}Co^{2+}$) uptake of the mutants can be directly compared with that of wild type. However, this can only be interpreted as a semi-quantitative comparison of channel function, not as a measure of absolute rate. For mutants that gave good levels of $^{63}Ni^{2+}$ uptake in comparison to wild type, no further analysis was performed. For mutants that gave low levels of $^{63}Ni^{2+}$ uptake relative to wild type or for mutants with significant amounts of protein in the inclusion body fraction, formaldehyde crosslinking of either membrane fractions or whole cells was performed, followed by SDS-PAGE and Western blotting. Previous work has demonstrated that formaldehyde crosslinking detects assembled CorA protein (40). All mutants tested showed assembly of oligomeric CorA in the membrane (Supplemental Figure 4 and data not shown). The transport experiments are a measurement solely of apparent cation affinity, not rate. This requires only that sufficient cpm of the radioisotope is taken up for accurate measurement and that CorA in the membrane is assembled (Supplemental Figure 4). Apparent cation affinity is completely independent of CorA protein level in the membrane and is not affected by the presence of CorA protein in

the inclusion body fraction. All strains expressing mutant CorA proteins were also tested for the ability to complement the growth of a Mg^{2+} dependent strain of *S.* Typhimurium (MM281). Most mutant CorA channels complemented growth as did wild type CorA, requiring no supplemental Mg^{2+} (data not shown). Those mutants that required supplemental Mg^{2+} for growth are discussed below.

Properties of the periplasmic loop

As the only part of CorA outside the cell, the periplasmic loop is presumably the first part of the protein to encounter Mg^{2+}. Several features of the loop are highly conserved across bacterial and archaeal species. The sequences of TM1-periplasmic loop-TM2 region of CorA are compared in Supplemental Figure 1 for CorA proteins related to the Enterobacteria *S.* Typhimurium (Supplemental Figure 1B), the thermophile *T. maritima* (Supplemental Figure 1C), and the archaeal Methanocaldococcus jannaschii (Supplemental Figure 1D) and are summarized in Supplemental Figure 1E. All three of these CorA channels give robust transport with essentially identical apparent cation affinities for all three substrate cations when expressed in *S.* Typhimurium ((42)and unpublished data). This supports comparison of *S.* Typhimurium transport data to the *T. maritima* structure as well as extension of this comparison across a wide range of CorA channels.

Figure 2 summarizes the conservation exhibited in the periplasmic loop. Position 1 of the loop is charged and position 2 is virtually always aromatic. Positions 3 to 6 are the highly conserved 'MPEL' motif. The proline in position 4 and the glutamic acid in position 5 are present in essentially all CorA channels. Position 7 is always charged, and position 8 is usually aromatic. Position 9 is variable but polar. Further, the charged residues at positions 1 and 7 are always oppositely charged, but the order of the charges (+/− *versus* −/+) is not conserved.

This high degree of conservation of the periplasmic loop implies an important role for these residues structurally and/or functionally. Negatively charged residues could directly bind cation, contributing to the cation selectivity of the channel. Alternatively, since positions 1 and 7 are always oppositely charged, a salt bridge between adjacent loops could provide structural stability. Conservation of aromatic residues could indicate base stacking and/or π-cation interactions between adjacent loops to help maintain structure. These general hypotheses provided a starting point for mutagenesis.

Conserved charge at positions 1 and 7 is not critical

Positions 1 and 7 are always oppositely charged, but their order varies. This argues that switching the order of the charges (an E281K K287E double mutant) would have little effect. Indeed, apparent cation affinity of the double mutant was identical to that of wild type (Figure 3A). A salt bridge would be disrupted if either residue were replaced with an oppositely charged residue. CorA channels with an E281K, E281R or E281D mutations or a K287E mutation demonstrated a modest decrease (right-shift) in apparent Mg^{2+} affinity of 2 to 4-fold (Figure 3A and 4A). These mutants all expressed similarly to wild type, and all gave a similar level of transport compared to wild type (Figure 3C). E281 could also be replaced with R, L, A or Q with no significant changes in apparent Mg^{2+} affinity (Figure 3B), again with transport rates near wild type levels (Figure 3C).

Likewise, at position 7, the lysine could be replaced with R, E or Q without affecting function significantly (Figures 3A and 4A), although apparent Mg^{2+} affinity was shifted about 10-fold to the right with K287 substitutions compared to about 3-fold with E281 substitutions. These results were not cation dependent as inhibition of $^{63}Ni^{2+}$ uptake of K287 mutants by Ni^{2+} and Co^{2+} gave similar results (Figures 4B and 4C). In contrast, dose

response curves for the inhibitor CoHex were shifted to the left, indicating an increase in apparent affinity for the inhibitor of about 10-fold (Figure 4D and data not shown). (The pattern of inhibition for the K287A and K287D mutants is discussed below.) All mutants inserted and assembled in the membrane giving uptake at least 60% of wild type (Supplemental Figures 2, 3 and 4 and data not shown). Thus, despite a high degree of evolutionary conservation, charge is not required at either position 1 or position 7 in the loop. This clearly shows that an electrostatic interaction of the Mg^{2+} cation with these residues plays no role in the channel's function.

E285 of the MPEL motif is functionally critical but not for its charge

The most conserved of the charged residues is E285 of the MPEL motif. E285 was mutated to D, Q, K, R and A. All mutants expressed at a level comparable to wild type and assembled in the membrane (Supplemental Figures 2, 3 and 4 and data not shown). However, none was functional in the standard transport assay. To try to detect an extremely low level of channel activity, E285 mutants were assayed using very high specific activity of radioisotope (10 μCi/tube *versus* ~0.3 μCi/tube). Apparent uptake in the presence of 50 mM Mg^{2+} was considered as background. The assay was performed using both $^{63}Ni^{2+}$ and $^{57}Co^{2+}$ to ensure that uptake was not cation dependent. At high specific activity, a low level of isotope uptake was detectable over background, approximately 0.3% that of wild type, except for E285D (Figure 5A and data not shown). As additional evidence of their ability to transport Mg^{2+}, E285 mutants were tested for complementation of growth in the Mg^{2+} dependent *S.* Typhimurium strain MM281. Strains expressing wild type or mutant CorA channels were grown in 96-well plates in N-minimal medium with various Mg^{2+} concentrations. MM281 with the empty vector requires >3 mM Mg^{2+} for growth while wild type CorA complements MM281 without added Mg^{2+} (Figure 5B). E285A and E285K must mediate Mg^{2+} uptake, as they were able to complement MM281 at less than 250 μM added Mg^{2+}. E285R and E285Q also complemented growth but required slightly higher Mg^{2+} concentrations. E285D, which showed no statistically significant uptake in the radioisotope assay, could complement growth, but required Mg^{2+} concentrations almost as high as MM281 transformed with empty vector. The order of Mg^{2+} dependence was WT < A < K < Q = R < D < empty vector. While these data indicate that E285 is critical for function, the ability of the E285A, E285K and E285R CorA channels to mediate very low levels of uptake and to complement growth argue that the negative charge of the glutamate at this position is not the determining property that explains its universal conservation.

An aromatic residue is required at position 8 but not 2

Aromatic residues at positions 2 and 8 are highly conserved in the periplasmic loop of CorA (Figure 2 and Supplemental Figure 1BCDE). Alternative residues at these positions are generally large and hydrophobic. The predominance of aromatic residues at these positions suggests the possibility of a base stacking interaction within or between monomers similar to that shown by the aromatic residues of the YGMNF motif (18). Surprisingly, at position 2, neither conservative mutations (F282Y or F282W) nor non-conservative mutations (F282A or F282C) had any effect on apparent Mg^{2+} affinity (Figure 6). All mutants exhibited levels of transport > 75% of wild type (Figure 6 insert). Indeed, F282C was the only Cys mutation in the loop to exhibit significant function. F282 therefore is not involved in base stacking and is not critical for function despite its conservation.

W288 mutants exhibited $^{63}Ni^{2+}$ uptake results considerably different from those of F282. While W288A and W288C mutants were expressed, W288A was non-functional in both transport and growth assays (data not shown). W288C showed a significant but minimal level of transport (Figure 7A). Conservative mutations, W288F and W288Y, gave levels of

transport approximately 15% of wild type. Thus, a tryptophan is required at position 8 in the loop for optimal transport.

Cooperative ion binding sites

Several mutant channels exhibited an anomalous pattern of uptake. K287A, K287D, W288Y and W288F all showed an increase in radioisotope uptake with increasing concentrations of nonradioactive inhibitory cation. Other mutations at these positions did not exhibit this pattern. This pattern of increased uptake occurred with all three substrate cations, Mg^{2+}, Ni^{2+} and Co^{2+} (Figure 4ABC and Figures 7BCD) for the K287A, K287D, W288Y channels. W288F showed a modest increase in uptake only in the presence of Co^{2+} (Figure 7C). All four mutants demonstrated decreases in apparent affinity for substrate cations up to ~100-fold. This pattern of transport has been previously observed for CorA carrying certain mutations in TM1 (25). Analysis of these mutants suggested significant positive cooperativity in cation interaction, indicating at least two distinct cation binding sites. The mutations would appear to decrease apparent affinity at or near the site of the mutation but not at a distinct and more distant site. As the mutated binding site is occupied at higher cation concentrations, flux increases through the channel. Further increases in cation concentration then give the expected pattern of inhibition as specific activity of the radioisotope decreases. If this interpretation is correct, the increase in uptake in the presence of inhibitory cation should not occur if inhibition is assayed at higher Ni^{2+} concentrations, where all binding sites would have significant occupancy. As predicted, the increases in $^{63}Ni^{2+}$ uptake with increasing Mg^{2+} concentrations was abolished at high Ni^{2+} concentrations (Figure 8).

Discussion

The high degree of sequence conservation of the periplasmic loop of the CorA Mg^{2+} channel (Supplemental Figure 1) indicates its importance for the structure and/or function of the channel. The structure of this region is unresolved in the three current crystal structures of CorA (18–20). This is interpreted to mean that the loop is flexible and mobile. As the only residues outside the extracellular membrane face, the loop would be expected to be the initial portion of the channel that encounters substrate cation and therefore is likely involved in cation recognition and selectivity. Characterization of the loop's function must take into account several factors. First, in the vast majority of CorA Mg^{2+} channels, the loop is charged and aromatic. These properties intuitively suggest that the loop residues would directly interact with Mg^{2+} and the other substrate cations, Ni^{2+} and Co^{2+} Interpretation of possible interactions must also consider that CorA recognizes both di- and tri-valent cations (31). Second, some CorA homologs have a loop sequence lacking charge and/or aromatic residues, *e.g., Methanocaldococcus jannaschii* CorA ((42) and Supplemental Figure 1D). Third, CorA appears to recognize a fully hydrated Mg^{2+} cation, not a partially or completely dehydrated cation (31). The differences in volume of the hydrated and atomic states of Mg^{2+} are significant. Even if the channel transported a partially rather than fully hydrated cation, the volume difference would still be substantial. Fourth, there is a symmetry mismatch between a homopentameric channel and a strictly hexacoordinate cation. Finally, the eukaryotic homolog of CorA, Mrs2, has a surprisingly high conductance (29), faster than the kinetics of Mg^{2+} water exchange would appear to allow. Preliminary data on *S.* Typhimurium CorA shows a similarly high conductance (C. Obejero-Paz, A. Moomaw, S.W. Jones and M.E. Maguire, unpublished). These properties suggest that the underlying chemistry of Mg^{2+} interaction with the CorA channel and its homologues is different from the well-established chemistry of Mg^{2+} interaction with enzymes and ATP (26).

Electrostatic interaction of Mg^{2+} and the periplasmic loop

Although the periplasmic loop has highly conserved glutamate and/or aspartate residues, the very fast conductance of CorA indicates that frank electrostatic interactions of Mg^{2+} with the carboxyl groups cannot occur. A Mg^{2+} ion bound to a single glutamate (or aspartate) would typically exhibit an affinity of ~5 mM; binding with 2 or more of the 10 glutamates in the *S.* Typhimurium loop would result in a binding constant well under 1 mM (26;32). Assuming a forward rate constant (k_1) equal to Mg^{2+}'s diffusion coefficient, an affinity of even 1 mM equates to a dissociation rate constant (k_{-1}) of 10^5/sec, 100–1000 times too slow for a conductance of ~100 pS. Thus, conservation of charge in the extracellular loop must involve structural constraints, not charge. These expectations are borne out by the mutagenesis studies at positions 1 and 7. If both positions are positively charged (E281K), negatively charged (K287E), or reversed in charge (E281K K287E), expression and levels of transport are minimally affected. The single mutants exhibit a decrease in apparent cation affinity of 3- to 10-fold; the double mutant is identical to wild type. The glutamate at position 5 is universally conserved. Mutation to any of several amino acids almost completely abolishes function. Nonetheless, mutation to A and K gives a more functional channel than mutation to D, which retains the negative charge. Thus, direct electrostatic interaction of cation with the loop does not occur.

Cooperative Mg^{2+} binding sites

Although electrostatic interactions do not occur, mutagenesis at loop positions 7 and 8 indicates that these residues form all or part of a site of Mg^{2+} interaction. Substitutions at these positions with residues similar in size to the wild type residue have marked effects on levels of transport and exhibit modest decreases in apparent cation affinity. However, K287D, K287A, W288F and W288Y mutants represent substitutions with smaller amino acids. Transport data for these mutants reveals a pattern of cation interaction indicative of apparent positive cooperativity, suggesting that the hydrated Mg^{2+} may be directly interaction with K287 and W288. The cooperativity presumably arises from interaction with this periplasmic loop binding site and at least one additional Mg^{2+} sites within the channel pore. The crystal structures of *T. maritima* CorA showed density within the pore centered on residue G309 (18–20). This residue is the equivalent of S274 in *S.* Typhimurium CorA. Our published transport data analyzing S274 and P278 mutations gave similar positively cooperative effects (25), indicative of a second Mg^{2+} interaction site. Molecular dynamic simulations (23) of *T. maritima* CorA with and without Mg^{2+} bound at the cytosolic metal binding sites indicated a cavity within the pore, centered on G309, that is of sufficient size to accommodate a partially and possibly a fully hydrated Mg^{2+}. Whether additional Mg^{2+} interaction sites with the loop or pore residues exist cannot be determined from these data.

The mutations at loop positions 7 and 8 would appear to decrease apparent affinity for cation at or near the site of the mutation but not at a distinct site some distance away. In the wild type channel, as Mg^{2+} binds to each site, ion repulsion presumably helps force the distal cation through the pore in the direction determined by the membrane potential. Mutation, by lowering cation affinity for one site, decreases occupancy at low concentrations, minimizing ion-ion interaction. As cation concentration increases, the site is filled, restoring ion-ion interaction, leading to repulsion and an increased rate of flux.

Ion flux involving ion-ion repulsion within the pore seems to be a common feature of ion channels (43) and has been observed particularly with Ca^{2+} and K$^+$ (44–50). The same phenomenon has been observed with the Na$^+$,K$^+$-ATPase transporter (51). Mutation of E327 in rat α$_2$- Na$^+$,K$^+$-ATPase apparently affects one (or two) K$^+$ binding sites on the external side. The data were interpreted to indicate positive cooperativity, where the site with weakened affinity must be filled for optimal transport. Facilitation of ion flux by occupancy

of successive cation binding sites has been demonstrated with other ion channels, *e.g.,* KcsA (52) and has been proposed previously for CorA (19).

Hydrated and dehydrated Mg^{2+}

Previous work identified CoHex and similar compounds as inhibitors of the CorA Mg^{2+} channel. CoHex has a diameter of approximately 5 and is thus a chemical analog of the hydrated Mg^{2+} ion. The ability of these cation hexaammines to inhibit CorA strongly suggests that the channel recognizes and binds a fully hydrated Mg^{2+} ion. Both crystallographic data and molecular dynamics simulations support the presence of a partially or fully hydrated Mg^{2+} near or at the upper end of the pore (19;23).

However, passage of a fully hydrated Mg^{2+} through the channel pore would require a pore diameter greater than 8Å and likely lead to a complete lack of cation selectivity. Consequently, a mechanism must exist for removing at least some waters of hydration from Mg^{2+} outside of or near the entrance to the pore. Further, these interactions must somehow facilitate or accelerate dehydration since the conductance of the channel appears to be at least two orders of magnitude greater than the rate of water exchange in the Mg^{2+} hydration shell.

Hypothesis

These disparate results might be reconciled if the periplasmic loop of CorA functions as a selectivity filter through interaction with the cation's hydration shell, rather than with the cation itself. By interacting with water, the amino acids of the loop would accelerate the dehydration necessary for the cation entry into the pore and achieve a very high rate of flux. Such an interaction could help explain the high selectivity of Mg^{2+} over other physiologically relevant cations. Mg^{2+} and the other two substrate cations Ni^{2+} and Co^{2+}, exchange water at a significantly slower rate than other common biological ions such as Ca^{2+}, Mn^{2+}, Na$^+$ and K$^+$ (Figure 1). While other hydrated ions could interact with the loop, their smaller size and extremely fast dehydration (and rehydration) rate would not allow a transient productive interaction. A somewhat similar mechanism has been proposed for the KcsA K$^+$ channel, where it has been suggested that selectivity for K$^+$ over Na$^+$ derives in part from the slightly slower dehydration rate of Na$^+$ (53). The difference in the role of hydration in the KcsA model and this CorA model is that the periplasmic loop of CorA is proposed to *accelerate* the rate of dehydration.

Analysis of the periplasmic loop has been reported for the *T. maritima* CorA Mg^{2+} channel and the expressed membrane domain of *Mycobacterium tuberculosis* CorA (54;55). Payandeh *et al*. generated an equivalent E to A mutation in the MPEL motif of the *T. maritima* CorA. That mutant also weakly complemented the growth of the Mg^{2+} deficient *Salmonella* strain MM281. Hu *et al*. used NMR spectroscopy to study a truncated version of the *M. tuberculosis* CorA composed of the two transmembrane segments and the connecting periplasmic loop. After reconstitution in detergent, this fragment forms a homopentamer, as with CorA. Chemical shifts of residues in the loop were measured by ^{1}H^{15}N HSQC in the presence and absence of ligands and inhibitors. The spectra suggested very weak binding of Mg^{2+}, Co^{2+} and CoHex to the glutamic acid of the MPEL motif (55). Hu *et al.* suggested that this weak interaction could involve a partially or completely hydrated cation. In both studies, the results were reasonably interpreted to suggest a chemistry whereby the glutamic acid acts as an electrostatic sink to concentrate ions near the pore of the channel. However, our data are not compatible with an interpretation involving electrostatic interaction at position E285 or elsewhere in the loop. As noted above, if the Mg^{2+} cation were to bind directly to the glutamic acid in the loop, the binding affinity would be too great to support the apparent conductance of the channel. Instead, results from the multiple substitutions at

E285 reported here are consistent with an interaction of this residue with a hydrated cation. In addition, the comparative effects of Mg^{2+}, Co^{2+} and CoHex interaction with the loop reported by Hu *et al.* (55) support the hypothesis that the hydrated cation is involved.

Interaction of the loop with a hydrated cation is also compatible with the results of mutation of the charged residues at positions 1 and 7. These positions are always of opposite charge, but their order varies. The ability of the K287E mutant to transport cation might be interpreted as due to an additional negative charge interacting with a cation. However, an E281K mutation leaves two positive charges in the loop, which could not directly interact with a cation. But the relatively normal function of this mutant can be explained if the residues at these positions interact with the fully hydrated cation since both positively and negatively charged residues would be able to interact with water.

The data presented here support a model where charged and aromatic periplasmic loop residues participate in dehydration of the substrate cation. The very slow rate of water exchange in the hydration shells of Mg^{2+}, Ni^{2+} and Co^{2+} apparently contributes to the selectivity of the CorA channel since the far more rapid water exchange rate of other cations would prevent a productive interaction. The glutamate in the MPEL motif does not interact electrostatically with Mg^{2+}, but nonetheless appears critical for function. A glutamate in this position might be required for optimal dehydration of the cation through precise effects on the structure of a transiently formed cation interaction site. While the loop must adopt a transient structure to interact productively with cation, the weakness of the interaction would not produce a sufficiently stable structure for detection by X-ray crystallography.

Such a model integrates the high conductance of Mg^{2+} channels with the slow dehydration rate of Mg^{2+} and with the symmetry mismatch of a pentameric channel and a hexacoordinate cation. It may also help explain the relative concentrations of the substrate cations required for half maximal uptake ($K_{0.5}$): Mg^{2+} (15 μM), Co^{2+} (20 μM) and Ni^{2+} (200 μM). The water exchange rates for Mg^{2+} and Co^{2+} are relatively similar but that for Ni^{2+} is almost 10-fold slower (Figure 1), implying that the channel would find it more difficult to accelerate dehydration of Ni^{2+} than of Mg^{2+} and Co^{2+}. As noted above, the model is also compatible with previous studies on the periplasmic loops of *T. maritima* and *M. tuberculosis* CorA. Finally, this model can explain the function of the few CorA periplasmic loops that do not closely follow the pattern described in Figure 2. For example, the CorA Mg^{2+} channel from the archaeal *Methanocaldococcus jannaschii* expresses well in *S.* Typhimurium. Cation uptake is virtually indistinguishable from the native CorA (42), including competitive inhibition by CoHex. Its periplasmic loop is SYLPLANNP (Supplemental Figure 1D), contains no charge and has homology with *S.* Typhimurium CorA only at positions 2–4. Direct electrostatic interaction with Mg^{2+} is clearly not possible, as has been noted (20;54). However, interaction of the *M. jannaschii* loop residues with a hydrated Mg^{2+} or with its CoHex analog is quite feasible. The results reported above show that the absence of charged residues in the periplasmic loop does not preclude functional interaction with cation.

Finally, this model supports the idea that channel opening is controlled by the Mg^{2+} binding sites between monomers in the cytosolic domain of the channel, not by cation interaction with the extracellular portion of the channel. A weak and transient cation interaction with the loop would be unlikely to trigger opening of the channel. If, however, the Mg^{2+} ions bound in the cytosolic domain sense a decrease in cytosolic Mg^{2+} concentration, their dissociation could trigger a conformational change that opens the pore as recently shown by Chakrabarti *et al*. (23). Thus, there is no necessity for the cation binding sites in the periplasmic loop (or pore) to control opening. Instead, the loop residues would only be required to generate the cation selectivity of the channel.

Supplementary Material

Refer to Web version on PubMed Central for supplementary material.

Abbreviations are

CoHex	cobalt(III)hexaammine trichloride
EDTA	ethylenediaminetetraacetic acid
LB	Luria broth
OD$_{600nm}$	optical density at 600 nm
TM	transmembrane segment

References

1. Cowan JA. Metallobiochemistry of Magnesium. Coordination Complexes with Biological Substrates: Site Specificity, Kinetics and Thermodynamics of Binding, and Implications for Activity. Inorganic Chemistry. 1991; 30:2740–2747.

2. Cowan JA. Metal activation of enzymes in nucleic acid biochemistry. Chem Rev. 1998; 98:1067–1087. [PubMed: 11848925]

3. Cowan JA, Ohyama T, Howard K, Rausch JW, Cowan SM, Le Grice SF. Metal-ion stoichiometry of the HIV-1 RT ribonuclease H domain: evidence for two mutually exclusive sites leads to new mechanistic insights on metal-mediated hydrolysis in nucleic acid biochemistry. J Biol Inorg Chem. 2000; 5:67–74. [PubMed: 10766438]

4. Dann CE III, Wakeman CA, Sieling CL, Baker SC, Irnov I, Winkler WC. Structure and mechanism of a metal-sensing regulatory RNA. Cell. 2007; 130:878–892. [PubMed: 17803910]

5. Quigley GJ, Teeter MM, Rich A. Structural analysis of spermine and magnesium ion binding to yeast phenylalanine transfer RNA. Proc Natl Acad Sci U S A. 1978; 75:64–68. [PubMed: 343112]

6. Shechter M, Shechter A. Magnesium and myocardial infarction. Clin Calcium. 2005; 15:111–115. [PubMed: 16272621]

7. Chubanov V, Schlingmann KP, Waring J, Heinzinger J, Kaske S, Waldegger S, Schnitzler MM, Gudermann T. Hypomagnesemia with secondary hypocalcemia due to a missense mutation in the putative pore-forming region of TRPM6. J Biol Chem. 2007; 282:7656–7667. [PubMed: 17197439]

8. Huang CL, Kuo E. Mechanism of hypokalemia in magnesium deficiency. J Am Soc Nephrol. 2007; 18:2649–2652. [PubMed: 17804670]

9. Muller D, Kausalya PJ, Meij IC, Hunziker W. Familial hypomagnesemia with hypercalciuria and nephrocalcinosis: blocking endocytosis restores surface expression of a novel Claudin-16 mutant that lacks the entire C-terminal cytosolic tail. Hum Mol Genet. 2006; 15:1049–1058. [PubMed: 16501001]

10. Champagne CM. Magnesium in hypertension, cardiovascular disease, metabolic syndrome, and other conditions: a review. Nutr Clin Pract. 2008; 23:142–151. [PubMed: 18390781]

11. Laires MJ, Monteiro CP, Bicho M. Role of cellular magnesium in health and human disease. Front Biosci. 2004; 9:262–276. [PubMed: 14766364]

12. Durlach J, Pages N, Bac P, Bara M, Guiet-Bara A. Magnesium deficit and sudden infant death syndrome (SIDS): SIDS due to magnesium deficiency and SIDS due to various forms of magnesium depletion: possible importance of the chronopathological form. Magnes Res. 2002; 15:269–278. [PubMed: 12635883]

13. Hmiel SP, Snavely MD, Florer JB, Maguire ME, Miller CG. Magnesium transport in *Salmonella typhimurium*: Genetic characterization and cloning of three magnesium transport loci. J Bacteriol. 1989; 171:4742–4751. [PubMed: 2548998]

14. Snavely MD, Gravina SA, Cheung TT, Miller CG, Maguire ME. Magnesium transport in *Salmonella typhimurium*: Regulation of *mgtA* and *mgtB* expression. J Biol Chem. 1991; 266:824–829. [PubMed: 1898738]

15. Snavely MD, Miller CG, Maguire ME. The *mgtB* Mg^{2+} transport locus of *Salmonella typhimurium* encodes a P-type ATPase. J Biol Chem. 1991; 266:815–823. [PubMed: 1824701]

16. Knoop V, Groth-Malonek M, Gebert M, Eifler K, Weyand K. Transport of magnesium and other divalent cations: evolution of the 2-TM-GxN proteins in the MIT superfamily. Mol Genet Genomics. 2005; 274:205–216. [PubMed: 16179994]

17. Maguire ME. The Structure of the CorA Magnesium Transporter, a Divalent Cation Channel. Curr Opin Struct Biol. 2006; 4:432–438. [PubMed: 16828282]

18. Lunin VV, Dobrovetsky E, Khutoreskaya G, Zhang R, Joachimiak A, Doyle DA, Bochkarev A, Maguire ME, Edwards AM, Koth CM. Crystal structure of the CorA Mg^{2+} transporter. Nature. 2006; 440:833–837. [PubMed: 16598263]

19. Payandeh J, Pai EF. A structural basis for Mg^{2+} homeostasis and the CorA translocation cycle. EMBO J. 2006; 25:3762–3773. [PubMed: 16902408]

20. Eshaghi S, Niegowski D, Kohl A, Martinez MD, Lesley SA, Nordlund P. Crystal structure of a divalent metal ion transporter CorA at 2.9 angstrom resolution. Science. 2006; 313:354–357. [PubMed: 16857941]

21. Hattori M, Tanaka Y, Fukai S, Ishitani R, Nureki O. Crystal structure of the MgtE Mg^{2+} transporter. Nature. 2007; 448:1072–1075. [PubMed: 17700703]

22. Moomaw AS, Maguire ME. The Unique Nature of Mg^{2+} Channels. Physiology. 2008; 23:275–285. [PubMed: 18927203]

23. Chakrabarti N, Neale C, Payandeh J, Pai EF, Pomès R. An Iris-Like Mechanism of Pore Dilation in the CorA Magnesium Transport System. Biophysical Journal. 2010; 98:784–792. [PubMed: 20197031]

24. Ishitani R, Sugita Y, Dohmae N, Furuya N, Hattori M, Nureki O. Mg^{2+}-sensing mechanism of Mg^{2+} transporter MgtE probed by molecular dynamics study. Proc Natl Acad Sci U S A. 2008; 105:15393–15398. [PubMed: 18832160]

25. Szegedy MA, Maguire ME. The CorA Mg^{2+} transport protein of *Salmonella typhimurium*. Mutagenesis of conserved residues in the second membrane domain. J Biol Chem. 1999; 274:36973–36979. [PubMed: 10601252]

26. Maguire ME, Cowan JA. Mg^{2+} chemistry and biochemistry. Biometals. 2002; 15:203–210. [PubMed: 12206387]

27. Hille, B. Ionic channels of excitable membranes. 3. Sinauer; Sunderland, Mass: 2001.

28. Maguire ME. Magnesium transporters: properties, regulation and structure. Front Biosci. 2006; 11:3149–3163. [PubMed: 16720382]

29. Schindl R, Weghuber J, Romanin C, Schweyen RJ. Mrs2p forms a high conductance Mg^{2+} selective channel in mitochondria. Biophys J. 2007; 93:3872–3883. [PubMed: 17827224]

30. Hattori M, Iwase N, Furuya N, Tanaka Y, Tsukazaki T, Ishitani R, Maguire ME, Ito K, Maturana A, Nureki O. Mg^{2+}-dependent gating mechanism of the MgtE Mg^{2+} channel underlies Mg^{2+} homeostasis. EMBO J. 2009; 28:3602–3612. [PubMed: 19798051]

31. Kucharski LM, Lubbe WJ, Maguire ME. Cation hexaammines are selective and potent inhibitors of the CorA magnesium transport system. J Biol Chem. 2000; 275:16767–16773. [PubMed: 10748031]

32. Cowan, JA. The Biological Chemistry of Magnesium. VCH Publishers; New York, NY: 1995.

33. Vieira J, Messing J. New pUC-derived cloning vectors with different selectable markers and DNA replication origins. Gene. 1991; 100:189–194. [PubMed: 1905257]

34. Hmiel SP, Snavely MD, Miller CG, Maguire ME. Magnesium transport in *Salmonella typhimurium*: Characterization of magnesium influx and cloning of a transport gene. J Bacteriol. 1986; 168:1444–1450. [PubMed: 3536881]

35. Grubbs RD, Snavely MD, Hmiel SP, Maguire ME. Magnesium transport in eukaryotic and prokaryotic cells using magnesium-28 ion. Methods Enzymol. 1989; 173:546–563. [PubMed: 2674619]

36. Maguire, ME. Salmonella: Methods and Protocols. Schatten, H.; Eisenstark, A., editors. Humana Press; Totowa, NJ: 2007. p. 289-306.

37. Nelson DL, Kennedy EP. Magnesium transport in *Escherichia coli*. Inhibition by cobaltous ion. J Biol Chem. 1971; 246:3042–3049. [PubMed: 4928897]

38. Snavely MD, Florer JB, Miller CG, Maguire ME. Magnesium transport in *Salmonella typhimurium*: $^{28}Mg^{2+}$ transport by the CorA, MgtA, and MgtB systems. J Bacteriol. 1989; 171:4761–4766. [PubMed: 2670893]

39. Fraser PD, Misawa N, Linden H, Yamano S, Kobayashi K, Sandmann G. Expression in *Escherichia coli*, purification, and reactivation of the recombinant *Erwinia uredovora* phytoene desaturase. J Biol Chem. 1992; 267:19891–19895. [PubMed: 1400305]

40. Warren MA, Kucharski LM, Veenstra A, Shi L, Grulich PF, Maguire ME. The CorA Mg^{2+} Transporter is a Homo-Tetramer. J Bacteriol. 2004; 186:4605–4612. [PubMed: 15231793]

41. Smith RL, Szegedy MA, Walker C, Wiet RM, Redpath A, Kaczmarek ML, Kucharski LM, Maguire ME. The CorA magnesium transport protein of *Salmonella typhimurium*: Mutagenesis of conserved residues in the third transmembrane segment identifies part of a Mg^{2+} pore. J Biol Chem. 1998; 273:28663–28669. [PubMed: 9786860]

42. Smith RL, Gottlieb E, Kucharski LM, Maguire ME. Functional similarity between Archaeal and Bacterial CorA magnesium transporters. J Bacteriol. 1998; 180:2788–2791. [PubMed: 9573171]

43. Gouaux E, MacKinnon R. Principles of selective ion transport in channels and pumps. Science. 2005; 310:1461–1465. [PubMed: 16322449]

44. Obejero-Paz CA, Gray IP, Jones SW. Y^{3+} block demonstrates an intracellular activation gate for the α1G T-type Ca^{2+} channel. J Gen Physiol. 2004; 124:631–640. [PubMed: 15572343]

45. Obejero-Paz CA, Gray IP, Jones SW. Ni^{2+} block of $Ca_V3.1$ (α1G) T-type calcium channels. J Gen Physiol. 2008; 132:239–250. [PubMed: 18663132]

46. Gibor G, Yakubovich D, Peretz A, Attali B. External barium affects the gating of KCNQ1 potassium channels and produces a pore block via two discrete sites. J Gen Physiol. 2004; 124:83–102. [PubMed: 15226366]

47. Kuo CC, Hess P. Ion permeation through the L-type Ca2+ channel in rat phaeochromocytoma cells: two sets of ion binding sites in the pore. J Physiol. 1993; 466:629–655. [PubMed: 8410710]

48. Gouaux E, MacKinnon R. Principles of selective ion transport in channels and pumps. Science. 2005; 310:1461–1465. [PubMed: 16322449]

49. Domene C, Vemparala S, Furini S, Sharp K, Klein ML. The role of conformation in ion permeation in a K+ channel. J Am Chem Soc. 2008; 130:3389–3398. [PubMed: 18293969]

50. Lockless SW, Zhou M, MacKinnon R. Structural and thermodynamic properties of selective ion binding in a K+ channel. PLoS Biol. 2007; 5:e121. [PubMed: 17472437]

51. Tepperman K, Millette LA, Johnson CL, Jewell-Motz EA, Lingrel JB, Wallick ET. Mutational analysis of Glu-327 of Na^+-K^+-ATPase reveals stimulation of $^{86}Rb^+$ uptake by external K^+ Am J Physiol. 1997; 273:C2065–C2079. [PubMed: 9435514]

52. Doyle DA, Morais Cabral J, Pfuetzner RA, Kuo A, Gulbis JM, Cohen SL, Chait BT, MacKinnon R. The structure of the potassium channel: molecular basis of K^+ conduction and selectivity. Science. 1998; 280:69–77. [PubMed: 9525859]

53. Noskov SY, Roux B. Importance of hydration and dynamics on the selectivity of the KcsA and NaK channels. J Gen Physiol. 2007; 129:135–143. [PubMed: 17227917]

54. Payandeh J, Li C, Ramjeesingh M, Poduch E, Bear CE, Pai EF. Probing structure-function relationships and gating mechanisms in the CorA Mg^{2+} transport system. J Biol Chem. 2008; 283:11721–11733. [PubMed: 18276588]

55. Hu J, Sharma M, Qin H, Gao FP, Cross TA. Ligand binding in the conserved interhelical loop of CorA, a magnesium transporter from Mycobacterium tuberculosis. J Biol Chem. 2009; 284:15619–15628. [PubMed: 19346249]

56. Diebler H, Eigen M, Ilgenfritz G, Maass G, Winkler R. Kinetics and mechanism of reactions of main group metal ions with biological carriers. Pure Appl Chem. 1969; 20:93–115.
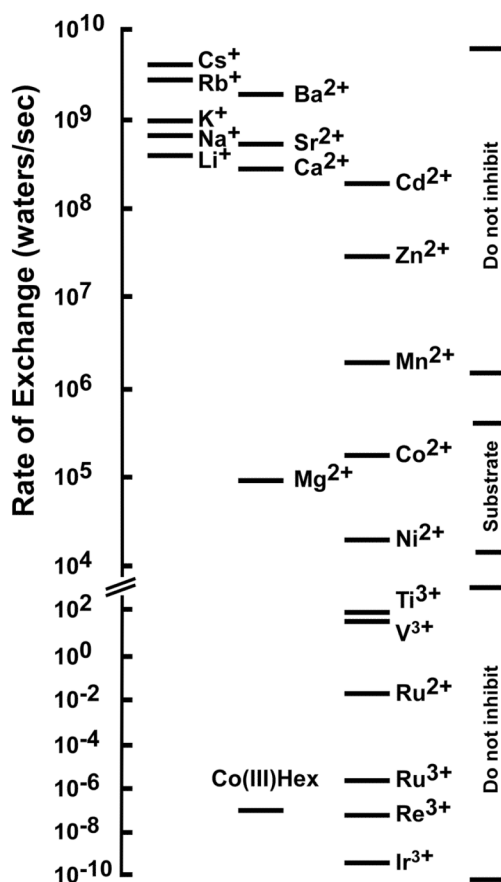
Figure 1. Water exchange rates for selected cations
Adapted from a similar figure in Hille (27) with additional data (56). The selective inhibitor of CorA, CoHex, is also shown; however, the exchange rate for CoHex is for the ammine groups, not water.
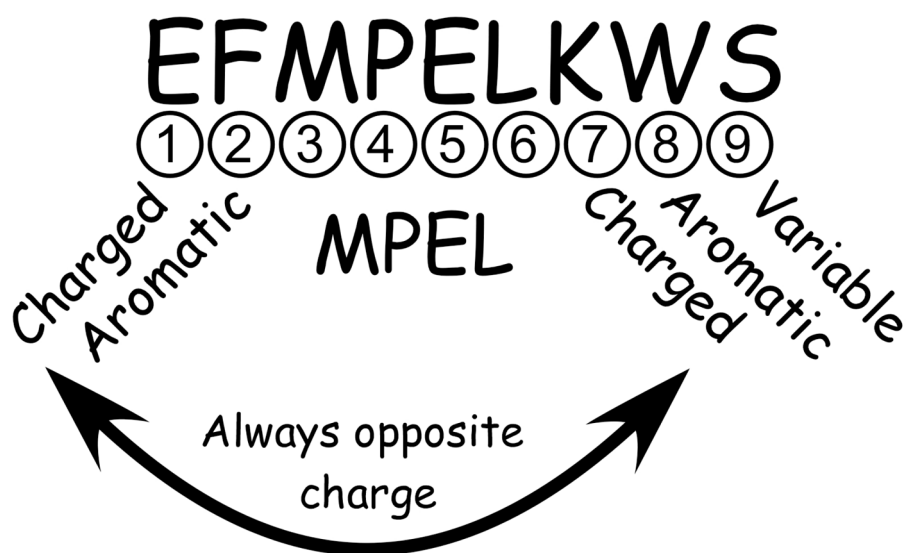
Figure 2. Properties of the periplasmic loop of the CorA Mg^{2+} channel
Conservation of amino acids at specific positions within the periplasmic loop is shown, based on the loop sequences shown in Supplemental Figure 1.
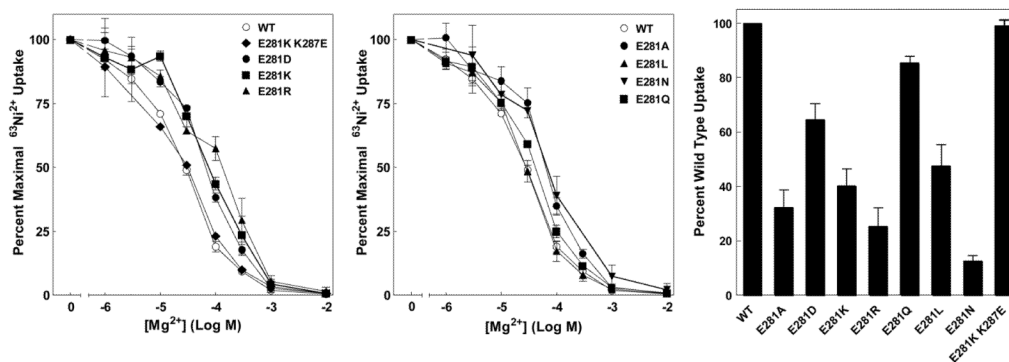
Figure 3. $^{63}Ni^{2+}$ uptake of E281 mutants
A. Mg^{2+} dose response curves for E281K, E281R, E281D single mutants and the E281K/K287E double mutant. B. Mg^{2+} dose response curves for E281A, E281L, E281N and E281Q single mutants. Each curve is normalized to maximal uptake for that strain in the absence of competing cation. The data are an average of at least 4 independent experiments done in triplicate. In a typical experiment, uptake ranged from 10,000 cpm for wild type to 1,500 cpm for E281N, over a background (10 mM Mg^{2+}) of ~600 cpm. C. Maximal $^{63}Ni^{2+}$ uptake determined by incubating cells for 10 min with ~0.3 μCi $^{63}Ni^{2+}$ per tube with a total $[Ni^{2+}]$ of 125 μM. Uptake in the presence of 10 mM Mg^{2+} (~600 cpm) was taken as background and subtracted from total uptake to give net cpm uptake. The data are representative of at least three independent experiments done in triplicate.
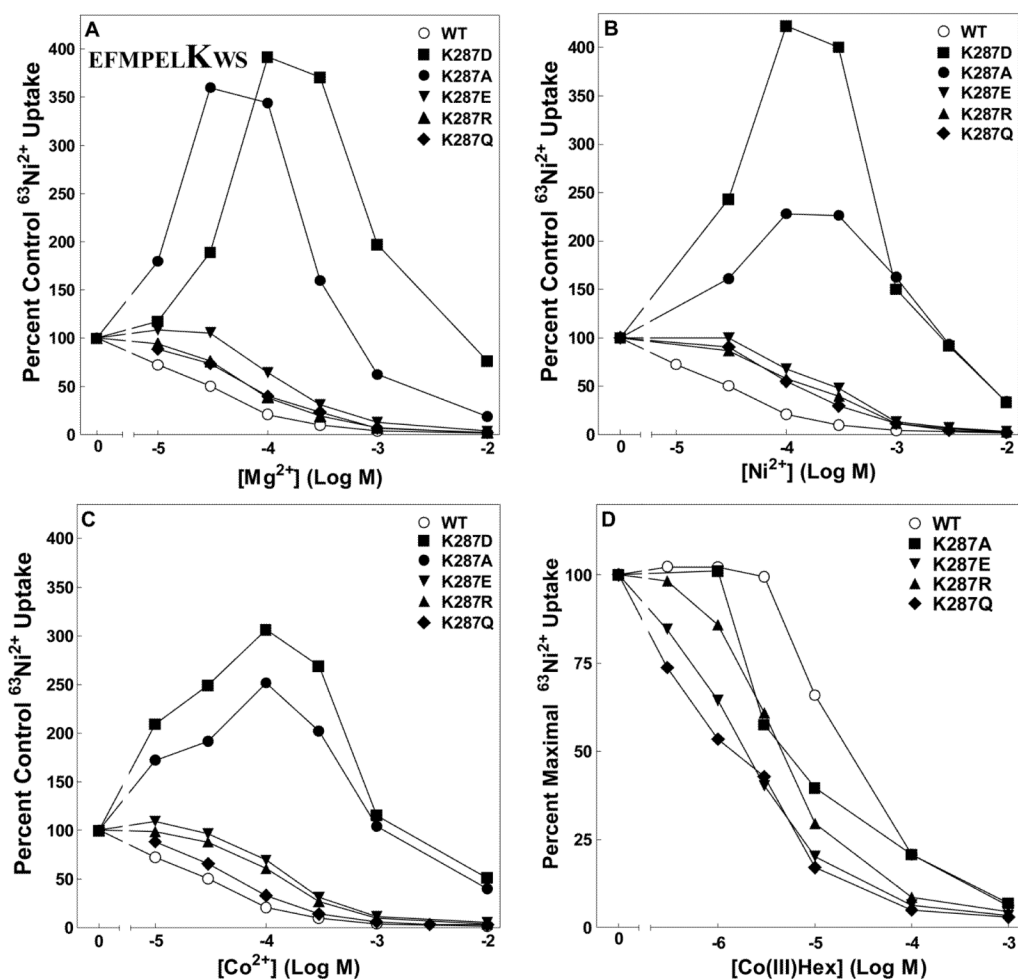
Figure 4. $^{63}Ni^{2+}$ uptake of K287 mutants
Dose response curves for K287D, K287A, K287E, K287R and K287Q mutants. Each curve is normalized to uptake for that strain in the absence of competing cation. A. Mg^{2+} dose response curve. B. Ni^{2+} dose response curve. C. Co^{2+} dose response curve. D. CoHex dose response curve. Data are representative of at least three independent experiments done in triplicate. In a typical experiment, uptake ranged from 30,000 cpm for wild type to 10,000 cpm for K287D, over a background (10 mM Mg^{2+}) of ~600 cpm. Error bars are not shown for clarity but were similar to those shown in Figure 3.
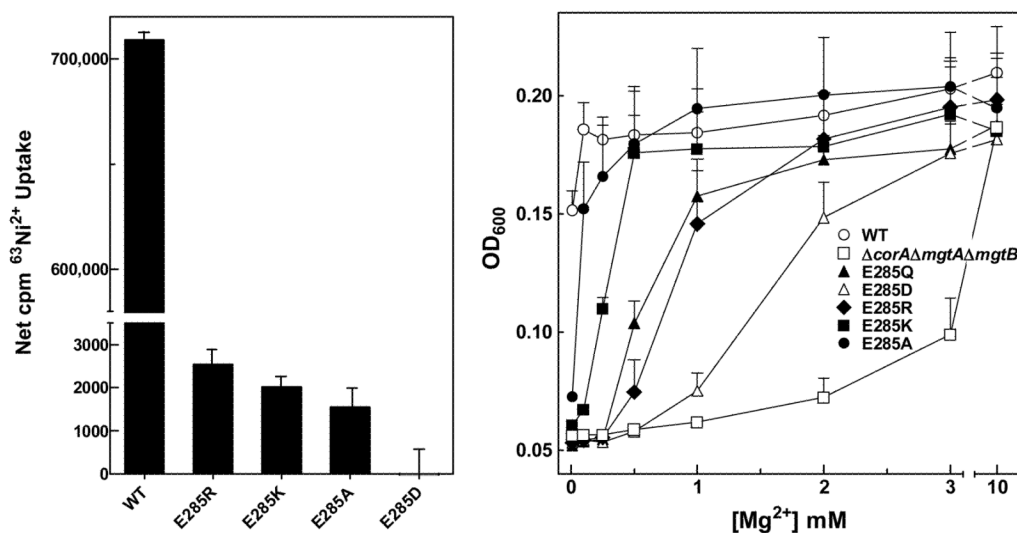
Figure 5. Analysis of E285 mutants

A. Maximal $^{63}Ni^{2+}$ uptake. Cells were incubated for 30 min with 10μCi $^{63}Ni^{2+}$ per tube with a total [Ni^{2+}] of 125 μM. Uptake in the presence of 50 mM Mg^{2+} (~1500 cpm) was taken as background and subtracted from total uptake to give net cpm uptake. The data are representative of at least two independent experiments with each mutant done in triplicate. B. Growth complementation of MM281 by E285 mutants. As described in *Methods*, OD_{600nm} was measured every 20 min for 14 hr. The data presented are at 6 hr growth and are representative of three independent experiments done in triplicate. For clarity, error bars are drawn in one direction only.
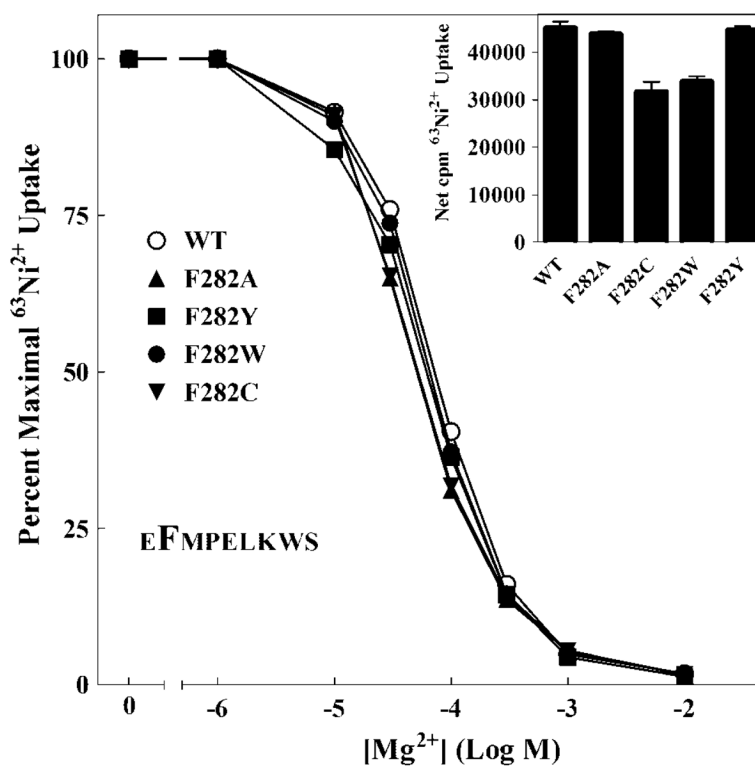
Figure 6. $^{63}Ni^{2+}$ uptake of F282 mutants
The Mg^{2+} dose response curves for F282A, F282C, F282W and F282Y single mutants shown. Each curve is normalized to uptake for that mutant in the absence of competing cation. In a typical experiment, uptake ranged from 40,000 cpm for wild type to 25,000 cpm for F282C, over a background (10 mM Mg^{2+}) of 600 cpm. *Inset*: To determine maximal $^{63}Ni^{2+}$ uptake, cells were incubated for 10 min with ~0.3 μCi $^{63}Ni^{2+}$ per tube with total [Ni^{2+}] of 125μM. Uptake in the presence of 10 mM Mg^{2+} (~600 cpm) was taken as background and subtracted from total uptake to give net cpm uptake. The data are representative of at least two independent experiments done in triplicate. Error bars are not shown for clarity but were similar to those shown in Figure 3.
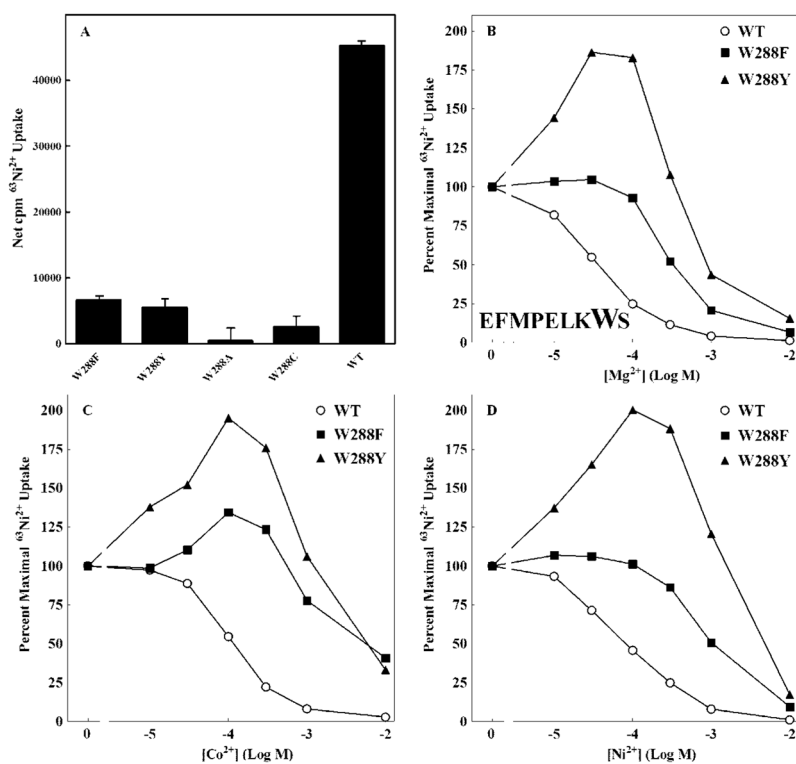
Figure 7. ^{63}Ni^{2+} uptake of W288 mutants
A. To determine maximal ^{63}Ni^{2+} uptake, cells were incubated for 10 min with 0.3 μCi ^{63}Ni^{2+} per tube with a total [Ni^{2+}] of 125μM. Uptake in the presence of 10 mM Mg^{2+} (~600 cpm) was taken as background and subtracted from total uptake to give net cpm uptake. The data are representative of at least two independent experiments done in triplicate. B. Mg^{2+} dose response curve. C. Co^{2+} dose response curve. D. Ni^{2+} dose response curve. Each curve is normalized to uptake for that mutant in the absence of competing cation. Data are representative of at least three independent experiments done in triplicate. Error bars are not shown for clarity but were similar to those shown in Figure 3. Maximal uptake for these mutants ranged from ~3,000 to 8,000 cpm.

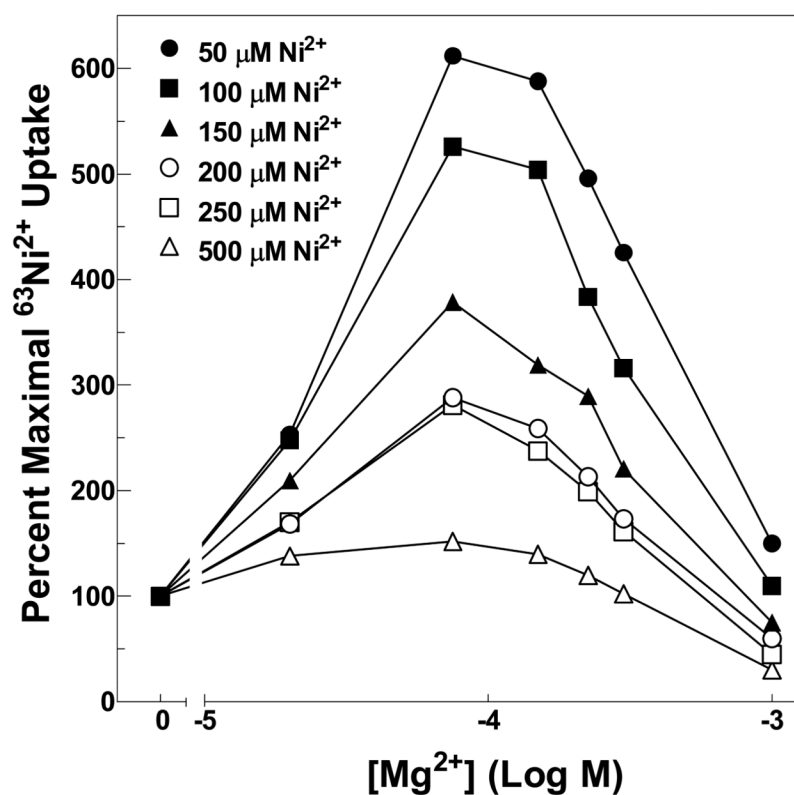**Figure 8. $^{63}Ni^{2+}$ uptake of the K287D mutant**
The ability of Mg^{2+} to inhibit $^{63}Ni^{2+}$ uptake was measured at different total Ni^{2+} concentrations. Each curve is normalized to uptake in the absence of competing cation at the indicated Ni^{2+} concentration. Data are representative of at least two independent experiments done in triplicate. Error bars are not shown for clarity but were similar to those shown in Figure 3. Maximal uptake for these mutants ranged from ~2,000 to 30,000 cpm.